Software and Hardware Prototype of IEEE 802.11ad Based Joint Radar Communication Transmitter

A THESIS

SUBMITTED IN PARTIAL FULFILLMENT OF THE REQUIREMENTS FOR

THE DEGREE OF

M.Tech

BY
Soumya Jain

Electronics and Communication Engineering
(Specialization - Communication and Signal Processing)

INDRAPRASTHA INSTITUTE OF INFORMATION TECHNOLOGY DELHI
NEW DELHI– 110020

July 28, 2022

Certificate

This is to certify that the thesis titled **"Software and Hardware Prototype of IEEE 802.11ad Based Joint Radar Communication Transmitter"** submitted by **Soumya Jain** for the partial fulfillment of the requirements of *Master of Technology in Electronics and Communications Engineering* is a record of the bonafide work carried out by her under my guidance and supervision at Indraprastha Institute of Information Technology, Delhi. This work has not been submitted anywhere else for the reward of any other degree.

Dr. Shobha Sundar Ram **Date: July 28, 2022**
Associate Professor
Dr. Sumit J Darak
Associate Professor
Department Of Electronics and Communication
Indraprastha Institute of Information Technology, Delhi

Acknowledgement

I would like to take this opportunity to express my sincere gratitude to the people who have supported me during my thesis work. Foremost, I would like to express my sincere gratitude to my advisors, Dr. Shobha Sundar Ram and Dr. Sumit J Darak, for their invaluable guidance, encouragement, and support throughout my thesis work. Their constructive feedback and regular work discussions helped me accomplish the task with great clarity. I would like to thank Dr. Niharika Agrawal for helping me with the tools and software. I would like extend my special thanks to Akanksha Sneh (Ph.D), V Sri Sindhu(M.Tech), Kshitiz Joshi(B.Tech) and Krisha Neel(B.Tech) for their collaboration with me on my thesis. Last but not least, I would like to thank my family and friends for supporting me through challenging times and for their guidance in managing my thesis work efficiently.

Abstract

Next-generation wireless communication systems are expected to support high-mobility and high-bandwidth vehicle-to-everything (V2X) communications in sub-6 GHz and millimeter wave (mmWave) spectrum. The deployment in mmWave spectrum demands rapid beam alignment of highly directional beams towards the mobile users to achieve the desired throughput. A potential solution investigated in this thesis is a joint radar-communication (JRC) system in the base station in which radar waveforms are embedded within the communication signal to enable accurate localization of the mobile user without the requirement of auxiliary sensors and spectrum. In this thesis, we propose a novel framework for a JRC transmitter based on the mmWave IEEE 802.11ad standard. Through the proposed system, we eliminate the lengthy beam alignment procedure in the standard IEEE 802.11ad protocol to realize shorter beam alignment durations. Next, we design a fixed-point synthesizable architecture of the proposed transmitter and verify its functionality on an FPGA platform. The performance studies of the word-length of the hardware implementation along with hardware IP cores for the transmitter form the third major contribution of the thesis.

Contents

List of Tables

List of Figures

Chapter 1: Introduction

1.1 Motivation

Next generation intelligent transportation systems (ITS) are expected to support high-mobility vehicle-to-everything (V2X) communication services to enhance information sharing related to the road environments to enhance road safety, and improved driving conditions eventually leading autonomous driving [1]. As per the current literature there are three modes of vehicular communications: *dedicated short-range communication services (DSRC)* on WLAN protocol IEEE 802.11p based technology [2]; *device-to-device long-term evolution (LTE)* based V2X communications (D2D-LTE V2X) [3] and *cellular LTE-V2X communications* [4]. All of these modes are designed for the sub-6 GHz spectrum, which provides data rates of tens of Megabits per second (Mbps) and latency of several hundred milliseconds (ms). However, the autonomous driving scenario requires sharing of real-time high definition 3D maps for sensing the environment in congested road conditions between vehicles, and it requires data rates of the order of Gigabits per second (Gbps) and ultra-low latency of the order of a few milliseconds.

Millimeter wave (mmW) unlicensed spectrum above 24 GHz, offers a solution for connected vehicles that require high bandwidths [5]. However, there are major challenges in the practical deployment of transceivers at the mmW spectrum. At such high carrier frequencies, the signal suffers high propagation loss and hence is required to operate in short-range line-of-sight (LOS) links enabled through highly directional beams using beamforming. Rapid beam training and management in a high mobility environment results in significant overhead, which in turn results in deterioration of latency [6]. Hence, auxiliary sensors such as GPS and radars are used to aid the beam alignment of the communication systems [7]. However, the addition of auxiliary sensors and radars increases the cost and complexity. Further, synchronization between two different types of systems is required and the mitigation of interference poses challenges. The mmW IEEE 802.11ad protocol in unlicensed spectrum offers a viable solution. However, the standard 802.11ad protocol incorporates a beamforming training protocol that searches for the best beam pair between the base station (BS) and mobile user (MU) through overheads in the PHY frame structure. This results in increased latency and decreased throughput. In this work, we propose to solve this problem by implementing a joint radar-communication transceiver to tackle the requirement of rapid beam alignment. Specifically, we embed radar functionality within the communications transceiver to enable rapid detection of mobile users and use the angular position estimates to direct the communication beams.

1.2 Objectives and Contributions

The main objective of the work presented in the thesis is to enable rapid beam alignment for V2X communication in mmWave spectrum without the requirement of additional spectrum and auxiliary sensors. In this work, IEEE 802.11ad standard physical layer (PHY) is studied with focus on packet format for the implementation of end-to-end architectures on hardware. The contributions of the thesis work are as follows:

1. Transmitter design based on integrating the radar functionality within IEEE 802.11ad communication protocol.
2. Timing analysis of proposed IEEE 802.11ad based JRC system with respect to standard IEEE 802.11ad.
3. Mapping of JRC transmitter design onto the FPGA platform for performance analysis using different word-lengths.

1.3 Literature Survey

JRC systems have been extensively researched in the last few decades. A comprehensive survey of the applications, feasibility, and advantages of JRC systems are presented in [8]. JRC research can be broadly categorised in three ways depending on the relation between the radar and communication functionalities [9]- *coexistence, cooperation and co-design*. The first category of works focus on the *coexistence* of radar and communications systems on a common spectrum where the main issue faced is RF congestion [10–13]. Hence these works focus primarily on the mitigation of mutual interference between the two systems with [11] or without cooperation [12]. In [10], the coexistence of MIMO communication system with a collocated MIMO radar system is discussed under a cooperative scenario where the physical layer information from both systems is shared at a control center and data fusion is performed for the radar systems. Here, transmit precoding is done to mitigate clutter and optimize the signal-to-interference plus noise (SINR) ratios. In [13], a spectrum sharing problem is formulated to keep radar as primary and WLAN as a secondary user in the spectrum and to analyze the effect of interference on throughput in WLAN as a function of distance. In the second category of JRC research, *passive radar* receivers are deployed with communication transmitters acting as opportunistic radar illuminators for remote sensing applications [14]. In both of the above two categories, the functionality of the two systems are not fully exploited as the systems are developed independently (with separate hardware). The third JRC approach explores *co-design* of the two systems. The work in [15] discusses radar-centric and communication-centric waveform design for JRC along with their parameters of evaluation. In this category, RF front ends are co-designed for sharing spectrum and hardware for both radar sensing, and communication [16, 17]. Here, one signal is embedded within the traditional framework of the other, i.e., the communication

signals are embedded within the radar waveform [18, 19] or the radar waveform are embedded within the communication signals [20]. In our work, we focus on the co-design of an IEEE 802.11ad based dual-functional full duplex transceiver that is capable of joint radar and communications operations.

Among the recent works in JRC, performance evaluation of communication and radar systems is discussed based on different metrics and their trade-offs to determine the optimum parameters for the joint operation of the two systems. In [21], the trade-off between communication data rates and radar estimation accuracy for a single target scenario is discussed for IEEE 802.11ad-based joint vehicular communication radar system. Beamforming is essential for directional communication, and codebook based MIMO beamforming for mmW WLAN is a fast and efficient method [22]. The discussion in [23] shows that the implementation of a fully digital JRC system is not feasible, and hence hybrid or analog beamforming is desirable. It also presents the machine learning approach that can be adopted for designing the JRC system. The authors in [24] present an analysis of IEEE 802.11ad based directional Wi-Fi communication with respect to the traditional Wi-Fi protocols. In [25], IEEE 802.11ad Wi-Fi router is designed to work as a base station as well as a radar in a vehicle-to-infrastructure (V2I) communication architecture. In [26], the performance of the communication system is evaluated using a novel parameter called *distortion MMSE or DMMSE* which is similar to Cramar-Rao lower bound (CRLB), where it explores the effect of signal-to-noise (SNR) ratio and the number of preambles required for efficient estimation of radar target velocity. In [27], the orthogonal frequency division multiplexing (OFDMA) and pulse modulated continuous wave (PMCW) waveforms are compared for JRC scenario using bistatic radars, and bit-error-rate (BER) and CRLB are the parameters used to evaluate the performance. In all the works mentioned above, the primary focus is the improvement in the algorithms and parameters. In our work, we focus on the end-to-end system design and analyze the time required to establish the directional link to enable reliable communication.

From the prototype perspective, there has been limited work in the design, prototype, and experimental demonstrations of co-designed multi-functional transceivers [28–30]. In [28], a spatial modulation based communication-radar system architecture was proposed with its hardware prototype, where individual radar and communications waveforms were realized with index modulation via generalized spatial modulation (GSM). Also, an array of transmitting antennas has been divided into two sub-arrays where one sub-array sends the radar signal, and the other sub-array sends the communication signal. In [29], a fully digital SIMO JRC architecture is designed on hardware where the target vehicle receives the communication signal from the source vehicle, and the radar signals are received by the source vehicle receiver. A hardware prototype is also developed in [30], where IEEE 802.11ay access points have been retrofitted for human detection and sensing in an indoor scenario. In [31], hardware-software co-design of IEEE 802.11a based physical layer transmitter is implemented on ZC706 and Zedboard with the re-usability of the blocks for other WLAN protocols including IEEE 802.11ad. To the best of our knowledge, there is no software or hardware prototype for an end-to-end IEEE 802.11ad based

JRC transceiver in the prior art.

1.4 Thesis Organisation

The thesis is organized as follows - Chapter 2 gives an overview of the end to end system architecture for standard IEEE 802.11ad and the proposed JRC. Chapter 3 gives the detailed description of the IEEE 802.11ad transmitter model. In Chapter 4, the fixed point HDL implementation of the transmitter model is explained. Chapter 5 shows the results for the time required for beam alignment for both standard and JRC architecture. This section also compares the results in floating point and fixed point architecture. Chapter 6 concludes the work and discusses the future scope

1.5 Notation

The notation used throughout the work is shown below in Table 1.1. Scalar variables are represented with regular face lower case letters while vectors are represented with boldface lower case letters and matrices are represented with boldface upper case letters. Furthermore, the symbol with the super-script as "(b)" as in $\mathbf{y}^{(b)}$ denoted the binary data in the form of bits. Vector superscript T and $*$ denotes transpose and complex conjugate respectively. We use the square braces, $[\cdot]$, to indicate discrete time sequences and the curly braces, $(\cdot)$, to indicate continuous time signals.

Table 1.1: Notations

Symbols	Representation
Radar signal	$\mathbf{x}$
Communication signal	$\mathbf{y}$
Signal undergone one-way propagation	$\hat{\mathbf{y}}$
Signal undergone two-way propagation	$\hat{\hat{\mathbf{y}}}$
Base station transmitter	BS-TX
Base station receiver	BS-RX
Mobile user transmitter	MU-TX
Mobile user receiver	MU-RX
Uni-directional communication between BS-TX and MU-RX	Downlink (DL)
Uni- directional communication between MU-TX and BS-RX	Uplink (UL)
Total number of OFDM symbols	N_{sym}
Number of antenna elements at transmitter	N_{TX}
Number of data sub-carriers in 1 OFDM symbol	N_{SD}
Single carrier (SC) sampling frequency	fs_{sc}
Bit period corresponding to SC	T_c
OFDM sampling frequency	fs_{OFDM}
Bit period corresponding to OFDM	T_s
Carrier frequency	f_c
Total samples in 1 OFDM symbol	T
Number of pilots in each OFDM symbol	N_p
Number of active sub-carriers $N_{SD} + N_p$	N_{Tones}
Guard interval duration	T_{GI}
Sub-carrier spacing	Δf
Duration of 1 OFDM symbol	T_{sym}
Windowing transition length	T_{TR}
Number of base station beams/BRF fields	M
Number of mobile user beams	N

Chapter 2: System Architecture

In this chapter, we discuss IEEE 802.11ad standard protocol with beam alignment for establishing directional communication between BS and MU along its end-to-end system architecture. We also propose the end-to-end system architecture for JRC in two versions and the timing required by two system architectures for determining the direction of the respective beams at BS and MU.

2.1 IEEE 802.11ad Standard Architecture

Directional communication links are required to overcome the atmospheric attenuation associated with mmW propagation. Hence, BS and MU must determine the best beams prior to $\mathbf{y}_{\mathrm{DL}}$ and $\mathbf{y}_{\mathrm{UL}}$ communication. The standard protocol utilizes In-packet training [32] using additional training fields within the packets for carrying out beam alignment. In our proposed work, the radar functionality at the BS is used for beam alignment instead to reduce the overall beam alignment time.
In this section, we present an overview of both the standard and the proposed JRC architectures and emphasize the modifications introduced in the former to realize the latter.
We begin by providing a brief description of the PHY layer of the IEEE 802.11ad packet structure [33]. Data and header transmission are enabled in three different modes: control, single carrier (SC), both at 1.76GHz sampling frequency, and orthogonal frequency division multiplexing (OFDM) mode at 2.64GHz sampling frequency as specified by the IEEE standard [33]. We model the data in our entire analysis in OFDM mode to enable high communication throughput and low latency. As shown in Fig.2.1, the packet consists of preamble, header, data, and BRF. The

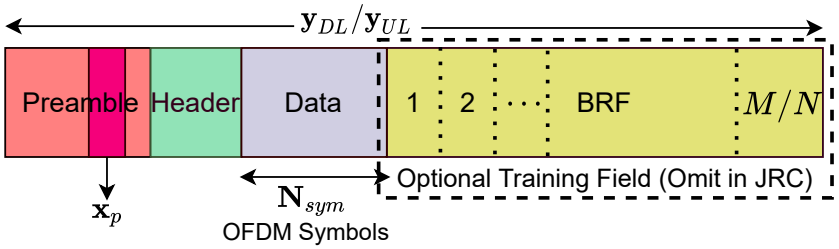

Figure 2.1: IEEE 802.11ad Transmit packet structure

preamble has Golay sequences that exhibit perfect auto-correlation properties (with zero sidelobes), which make them suitable for radar remote sensing and channel estimation for communication. The preamble is followed by a header which provides necessary control information to decode and demodulate the received data. The header is followed by data, after which BRF field with Golay sequences is provided for enabling beam training between BS and MU. The number of BRF fields has to be in multiples of 4 up to a maximum of 64 fields. In our proposed JRC ar-

chitecture, we omit these BRF fields as beam alignment is achieved through radar, as mentioned in the previous section. The wireless transceiver architecture for supporting standard 802.11ad communication is presented in Fig.2.2. The 802.11ad packets ($\mathbf{y}_{DL}$) are generated in the BS-TX and subsequently passed through the digital front end (DFE) consisting of a digital-to-analog converter (DAC). Subsequently,

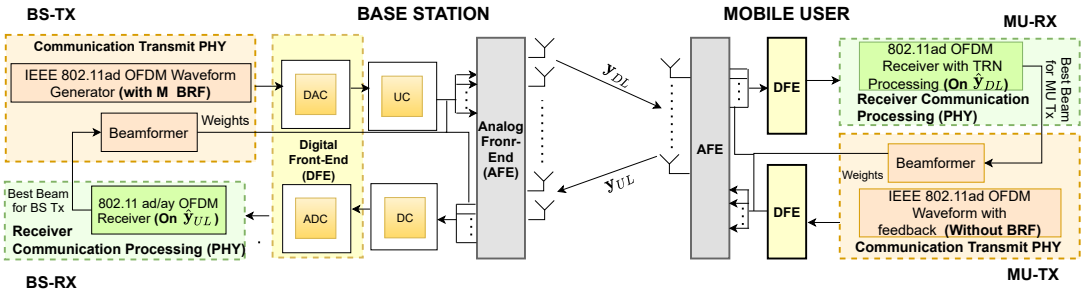

Figure 2.2: Standard IEEE 802.11ad system architecture

the analog signal is modulated with an RF carrier in the analog front end (AFE), amplified, and transmitted through a transmit phased antenna array. During the beam alignment phase, which we will henceforth refer to as *Stage 1*, the preamble, header, and data of the $\mathbf{y}_{\mathrm{DL}}$ packet are transmitted through a quasi-omnidirectional beam. M additional BRF fields are appended to the $\mathbf{y}_{\mathrm{DL}}$ packet and transmitted along the M possible beams supported by the BS-TX phased array. Suitable antenna weight vectors (AWV) are applied at the BS-TX phased array to steer each BRF along the corresponding beam direction. The received signal at the phased array on the MU-RX, $\hat{\mathbf{y}}_{DL}$, is down-converted, digitized, and processed to obtain the data. Based on the number of antennas in the MU-RX, N total beams may be supported through analog beamforming at the MU. Based on [32], the BS will repeat the transmission of the $\mathbf{y}_{\mathrm{DL}}$ packet N times, and each packet will be received sequentially by different beams at MU. The steps to determine the best beam for both BS and MU, i.e., the steps in *Stage-1* are described in Table. 2.1.

Table 2.1: Steps for analysing timing for standard architecture

Step 1	BS-TX sends $n = 1, 2 \cdots, N$ downlink packets with M BRF fields. Each of the m^{th} BRF fields is directed along m^{th} beam.
Step 2	MU-RX receives N packets from $n = 1, 2, \cdots, N$different beams.
Step 3	The $n = 1, 2, \cdots, N$ received packets are processed at MU-RX(RCP) sequentially. The BRF field processing determines $(\tilde{m}, \tilde{n})$ best beam pair.
Step 4	MU-TX sends $\mathbf{y}_{UL}$ with no BRF field over the $\tilde{n}^{th}$ beam with $\tilde{m}^{th}$ as feedback.
Step 5	The BS-RX receives $\mathbf{y}_{UL}$ and BS learns about its best beam ,i.e. $\tilde{m}$. This completes *Stage -1* for the standard architecture.

The pictorial representation of the above table is shown in the timing diagram in Fig.2.3. Hence, to summarize, the M training fields in the $\hat{\mathbf{y}}_{\mathrm{DL}}$ packet are received

through N beams of the MU-RX, leading to an overall complexity of $M \times N$. The best beam pair for the BS-TX and MU-RX will be estimated after the N packets are processed at the MU-RX. If we assume reciprocity in the propagation environment, then the beam alignment procedure between BS-TX and MU-RX for $\mathbf{y}_{\mathrm{DL}}$ will provide the necessary information to support the $\mathbf{y}_{\mathrm{UL}}$ communication between MU-TX and BS-RX (as the same antennas support both the TX and RX functionalities at both BS and MU). The total duration for the beam alignment is the duration of the N DL packets each appended with M training fields, the propagation time between the BS and MU, and the receiver communication processing (RCP) time at the MU. Once the beam alignment is completed and communicated to the BS, we enter *Stage 2*, where the data packets are transmitted between the BS and MU along the best beam pair without the need for BRF. The beam alignment process is repeated again depending on the mobility of the MU and the corresponding BER estimated at the BS and MU.

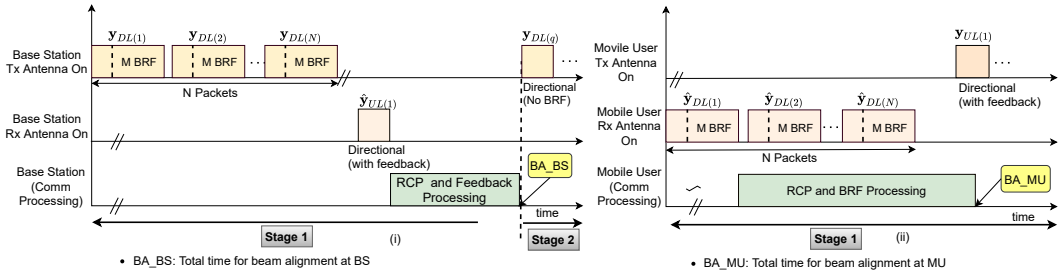

Figure 2.3: Timing diagram for *stage - 1* beam alignment based on beam training procedure

2.2 JRC Architecture

In this work, we introduce a JRC framework within the standard architecture at the BS, as shown in Fig.2.4, to reduce the latency caused by beam alignment as discussed above. During the beam alignment *Stage 1*, the transmitter at the BS-TX generates both radar ($\mathbf{x}_{\mathrm{p}}$) and communication waveforms ($\mathbf{y}_{\mathrm{DL}}$).

In prior art in [34, 35], the radar waveform was embedded within the communication packet. However, for short ranges typical of automotive environments ($\sim$40 to 200m), this results in very short two-way propagation times (of the order of several nanoseconds), which fall within the duration of the $\mathbf{y}_{\mathrm{DL}}$ packet (which is of several microseconds). Hence, the signal model suggested in the prior art would require a separate set of antennas (or additional mmW hardware) at the BS-TX and BS-RX to support the transmission of the $\mathbf{y}_{\mathrm{DL}}$ through BS-TX while receiving the radar scattered signal $\hat{\hat{\mathbf{x}}}_p$ from the MU at BS-RX. This architectural choice considerably increases the cost of the system. Further, the reciprocity in the propagation channels for $\mathbf{y}_{\mathrm{DL}}$ and $\mathbf{y}_{\mathrm{UL}}$ communications would no longer hold, and separate beam alignment procedures would have to be conducted for both $\mathbf{y}_{\mathrm{DL}}$ and $\mathbf{y}_{\mathrm{UL}}$. For both these reasons, we propose that a separate radar waveform composed of just a section of the 802.11ad

preamble is transmitted by BS-TX antennas through a quasi-omnidirectional beam. P pulses of the radar waveform, denoted by $\mathbf{x}_\mathrm{p}, p = 1 : P$, are transmitted at a pulse repetition interval of T_{PRI} as shown in the timing diagram for the JRC architecture presented in Fig. 2.5 and Fig. 2.6 . Due to the short duty cycle of the radar pulse with respect to the T_{PRI}, the same set of antennas can be used for both radar transmission at BS-TX and reception at BS-RX. We propose full duplex mode operation supported with advanced circulators, isolators, and self-interference cancellation systems [26]. The radar signals are upconverted from baseband to analog in the DFE and subse-

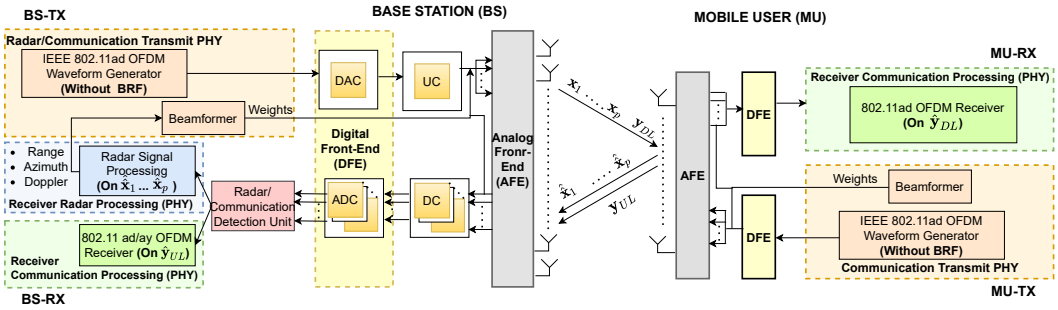

Figure 2.4: Proposed JRC system architecture with beam alignment of BS through radar signal processing and corresponding

quently to RF in the AFE. Since the radar waveform is composed of the 802.11ad packet preamble features, the same DFE and AFE and phased antenna array can be used for generating and transmitting both $\mathbf{x}_\mathrm{p}$ and $\mathbf{y}_\mathrm{DL}$. The transmitted signal $\mathbf{x}_\mathrm{p}$ scatters at the MU and is received at the BS-RX, where it is down-converted and digitized at the AFE and DFE. We introduce a radar-communication decision unit at the BS-RX for identifying scattered returns of $\hat{\hat{\mathbf{x}}}_p$ from the scattered $\hat{\mathbf{y}}_\mathrm{DL}$ and uplink packet $\hat{\mathbf{y}}_\mathrm{UL}$. The scattered $\hat{\hat{\mathbf{x}}}_p$ are processed at the radar signal processing unit (RSP), where the MU are detected based on their range returns, identified from static clutter based on their Doppler and subsequently located in the angular space. This information from the RSP is used as feedback to the beamformer to enable the alignment at the BS-TX and BS-RX during *Stage 2*. The total time required for the beam alignment at BS is, therefore, the duration of the P pulse repetition intervals ($P \times T_{PRI}$) and the radar signal processing time. Since these packets are considerably shorter than $\mathbf{y}_\mathrm{DL}$, the total duration for beam alignment is expected to be considerably lower than the standard. Note that in our proposed architecture, the RSP is introduced only in the BS and not in the MU. In other words, we have proposed digital beamforming at the BS-RX but retained analog beamforming at BS-TX, MU-TX, and MU-RX due to cost and complexity considerations. Hence, the beam alignment at the MU will be carried out as per the standard protocol. This architectural design choice is made since the number of beams at the BS are typically much greater than at the MU due to the higher number of antennas at the BS compared to the MU. We propose two versions for the beam alignment at the MU as shown in Fig. 2.5 and Fig .2.6.

2.2.1 JRC *Version-1*

In the *Version-1* for the JRC architecture, the MU sends a $\mathbf{y}_{\mathrm{UL}}$ packet with N BRF fields along the N possible beams. Then the best beam is determined at the BS-RX and subsequently communicated to the MU through the next $\mathbf{y}_{\mathrm{DL}}$. This is shown in Fig. 2.5.

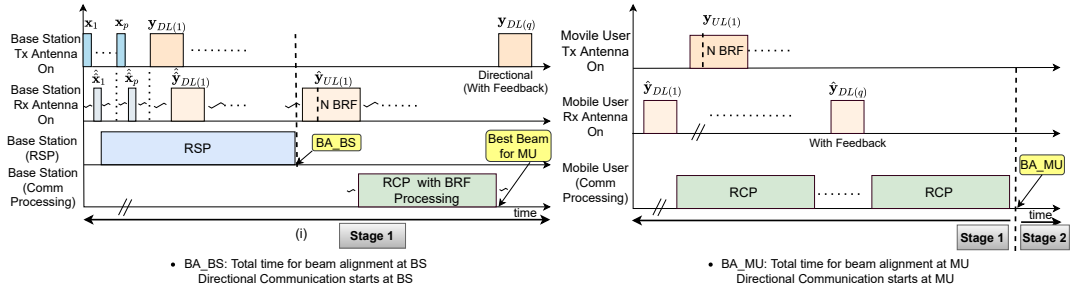

Figure 2.5: Timing diagram of JRC *Version-1* where beam alignment of MU is through longer uplink packet with multiple (N) BRF fields

The steps to analyse the time required to establish directional communication between BS and MU for is given in Table. 2.2. Thus, it can be summarised that the

Table 2.2: Steps for analysing timing for JRC *Version -1*

Step 1	BS-TX sends $\mathbf{x}_p$ which reflects from the MU and other targets in the environment.
Step 2	The received $\hat{\hat{x}}_p$ is passed through radar/comm detection unit and processed at BS(RSP). The azimuth of MU (θ_b) is determined at BS.
Step 3	BS-TX sends an quasi-omnidirectional $\mathbf{y}_{DL}$ with no BRF fields.
Step 4	The $\hat{\mathbf{y}}_{DL}$ is received and processed at MU-RX(RCP) for Simultaneously, the MU-TX sends the $\mathbf{y}_{UL}$ with N BRF fields.
Step 5	The received $\hat{\mathbf{y}}_{UL}$ is passed through radar/comm detection unit and processed at BS-RX(RCP). Best beam, $\tilde{n}^{th}$ is determined.
Step 6	The directional $\mathbf{y}_{DL}$ corresponding to θ_b is sent along with information regarding $\tilde{n}^{th}$ BRF field as feedback.
Step 7	Directional $\hat{\mathbf{y}}_{DL}$ is received and processed at MU-RX(RCP) and learn about $\tilde{n}^{th}$ BRF field and completes *Stage-1*.

total duration for beam alignment at the MU is based on the length of one long packet $\mathbf{y}_{\mathrm{UL}}$ with N BRF, propagation delay, and processing times at BS and MU.

2.2.2 JRC *Version-2*

The *Version-2* of the JRC architecture is shown in Fig.2.6, is similar to standard architecture as in Fig.2.3. Here, N $\hat{\mathbf{y}}_{\mathrm{DL}}$ packets are received along N beams at the MU to determine the best beam at MU.

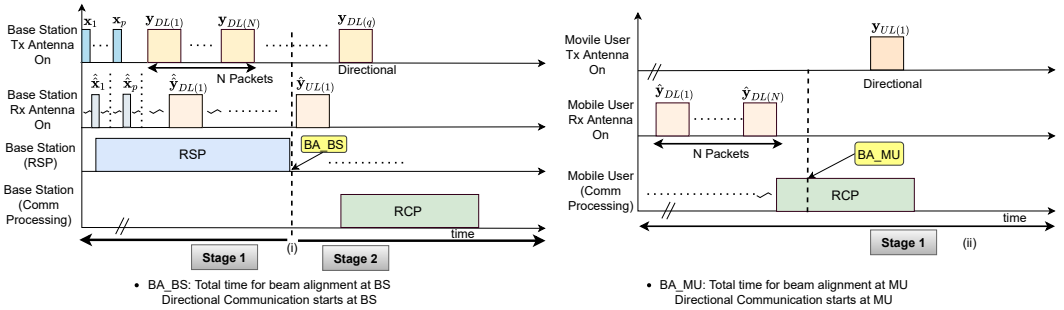

Figure 2.6: Timing for JRC *Version-2* where beam alignment of MU is through reception of multiple (N) downlink packets through separate MU beams.

The step-by-step analysis for time required for beam alignment in JRC architecture *Version-2* is given in Table. 2.3.

Table 2.3: Steps for analysing timing for JRC *Version-2*

Step 1	BS-TX sends $\mathbf{x}_p$ which reflects from the MU and other targets in the environment.
Step 2	The received $\hat{\hat{x}}_p$ is passed through radar/comm detection unit and processed at BS(RSP). The azimuth of MU (θ_b) is determined at BS.
Step 3	BS-TX sends $n = 1, 2, \cdots, N$ quasi-omnidirectional $\mathbf{y}_{DL}$ packets with no BRF fields.
Step 4	The $n = 1, 2, \cdots, N$ received $\hat{\mathbf{y}}_{DL}$ packets are processed at MU-RX(RCP). The correlation gain from preamble determines best beam, $\tilde{n}$.
Step 5	Since, RSP takes longer duration than determining the correlation gain from preamble, hence the *Stage-1* for *Version -2* is completed when the RPS is completed.

Thus, we can summarise that the duration of *Stage 1* is based on the duration to determine the correlation gains of preambles of N DL packets in *Version-2* along with the propagation time and the communication processing time. Again, since the time complexity is of the order of N rather than $M \times N$, we expect that the beam alignment will be quicker for the MU thereby supporting lower latency.

Hence, to conclude, the duration of the beam alignment stage for all three architectures is a function of the signal/packet lengths and the signal processing times. More details on the comparison of the timing values are provided in Chapter.5 with suitable examples.

Chapter 3: IEEE 802.11ad Transmitter Model

In this chapter, we provide a detailed discussion of the JRC signal model and the corresponding software prototype required to generate the signal at the transmitter.The parameters used are mentioned in Table 3.1. The hardware prototype of the same is explained in Chapter 4. The different blocks of the waveform generator within the transmitter are shown in Fig.3.1.

Table 3.1: Parameters for the Transmitter model

Parameters	Value
Number of data sub-carriers in 1 OFDM symbol (N_{SD})	336
Single Carrier (SC) Sampling Frequency (T_c)	1.76GHz
Bit period corresponding to SC (T_c)	1/fs$_{sc}$
OFDM Sampling Frequency (T_s)	2.64GHz
Bit period corresponding to OFDM (T_s)	1/fs$_{OFDM}$
Carrier Frequency (f_c)	60GHz
q^{th} OFDM symbol	1, 2, $\cdots$,N$_{sym}$
Total samples in 1 OFDM symbol (T)	640
Number of pilots in each OFDM symbol (N_p)	16
Number of active sub-carriers $(N_{SD} + N_p)$	352
Guard Interval Duration (T_{GI})	128/(2.64 $\times 10^9$)
Sub-carrier spacing (Δf)	(2.64 $\times 10^9$)/512
Duration of 1 OFDM Symbol (T_{sym})	0.242 μsec
Windowing Transition Length (T_{TR})	16

We will describe the generation of each part of the packet.

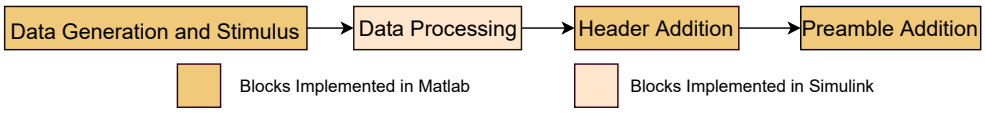

Figure 3.1: IEEE 802.11ad JRC waveform generation

3.1 Preamble and BRF Processing

Both the preamble and BRF fields are always SC modulated even when header and data fields are modulated with OFDM. The preamble is divided into the short training field (STF) and the channel estimation field (CEF) as shown in Fig.3.2. The STF consists of sixteen repetitions of 128-bit Golay sequences denoted by $\mathrm{g}_{a_{128}}$ followed by one repetition of $-\mathrm{g}_{a_{128}}$. The STF bits are phase-shifted by integer multiples of $\pi/2$ as shown in -

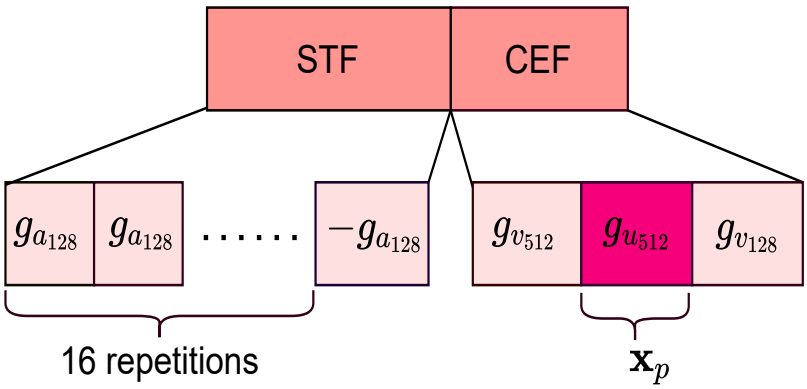

Figure 3.2: Expanded Preamble Structure

$$\mathbf{y}_{STF}[mT_c] = \begin{cases} \mathbf{g}_{a_{128}}[m\%128]exp(+j\frac{\pi}{2}m); \\ \qquad m = 0, 1, \cdots, 16 \times 128 - 1 \\ -\mathbf{g}_{a_{128}}[m\%128]exp(+j\frac{\pi}{2}m); \\ \qquad m = 16 \times 128 \cdots (17 \times 128) - 1. \end{cases} \tag{3.1}$$

Here, $\%$ indicates a modulus operation. The CEF consists of a 512-bit Golay complementary pair, denoted by $\mathbf{g}_{u_{512}}$ and $\mathbf{g}_{v_{512}}$ followed by a 128 bit Golay sequence denoted by $\mathbf{g}_{v_{128}}$ which are similarly modulated to

$$\begin{aligned} \mathbf{y}_{CEF}[mT_c] = &(\mathbf{g}_{u_{512}}[m] + \mathbf{g}_{v_{512}}[m - 512] + \mathbf{g}_{v_{128}}[m - 1024]) \\ &exp(+j\frac{\pi}{2}m); m = 0, 1, \cdots 1151. \end{aligned} \tag{3.2}$$

Together, they are concatenated to form the total preamble $\mathbf{y}_{mod}$. The sampling frequency for OFDM data bits is 2.64GHz which is 1.5 times that of SC used for preamble bits and hence up-conversion and down-conversion of the Golay sequences are required. First, the preamble bits are upsampled by a factor of three as shown below -

$$\mathbf{y}_{upsample}\left[m\frac{T_s}{2}\right] = \begin{cases} \mathbf{y}_{mod}[m\frac{T_c}{3}]; & m = 0, 3, 6 \cdots \\ 0; & \text{otherwise.} \end{cases} \tag{3.3}$$

The up-sampled signal is subsequently smoothened by a linear digital filter where $\mathbf{h}_{filt}[k], k = 1 \cdots K$ are the filter coefficients specified by the protocol [33] to obtain

$$\begin{aligned} \mathbf{y}_{filt}\left[m\frac{T_s}{2}\right] = \sum_{k=1}^{K} \mathbf{y}_{upsample}\left[(m-k)\frac{T_s}{2}\right]\mathbf{h}_{filt}[k], \\ m = 0, 1, \cdots 4992; k = 1, 2 \cdots K. \end{aligned} \tag{3.4}$$

Then the signal is downsampled by a factor of 2 to obtain

$$\begin{aligned} \mathbf{y}_{preamble}[mT_s] = \mathbf{y}_{filt}\left[2m\frac{T_s}{2} - \frac{K-1}{2}\frac{T_s}{2}\right] \\ m = 0, 1, \cdots 4992. \end{aligned} \tag{3.5}$$

The total length of $\mathbf{y}_{preamble}$ is 4992 samples, and it is of 1.89μs duration. The steps for generating the preamble bits are summarized in Fig.3.3. The radar waveform is generated using the CEF bits as indicated in Fig.3.2. Hence each p^{th} frame of the radar waveform corresponds to a uniquely generated $\mathbf{x}_{\mathrm{p}} = \mathbf{y}_{preamble}[4033 : 4800]$ consisting of $M' = 768$ samples. Since radar bits are already sampled at 2.64GHz, there is no need for sample rate conversion. Note that the radar waveform across consecutive T_{PRI} are not identical as they are generated from different seeds used for generating Golay complementary sequences.

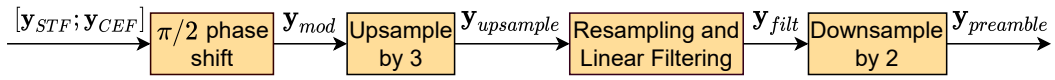

Figure 3.3: Preamble and BRF processing

The BRF fields are optional fields to be used when beam alignment is required. Each BRF consists of two sub-fields - automatic gain control (AGC) and training (TRN) fields - as shown in Fig.3.4. The AGC subfields consist of 64 bit Golay sequences, $\mathbf{g}_{a_{64}}$, repeated M times where M is the total number of beams supported by analog beamforming for the phased array in BS-TX. The BRF fields consist of the CEF followed by complementary 128 bit Golay sequences, $\mathbf{g}_{a_{128}}$ and $-\mathbf{g}_{b_{128}}$, arranged as shown in Fig.3.4 and replicated $M/4$ times. The CEF in the BRF is identical to the CEF in the preamble. The bits in the BRF are generated at a chip duration of T_c and subsequently processed in a manner identical to the preamble as shown in Fig.3.3 to obtain $\mathbf{y}_{BRF}$. Their total duration can be calculated as $2.290 \times [(M/4)]\mu s$. In the proposed JRC architecture, these fields are not needed and skipped during *Stage 1*. In the standard architecture, these are used in *Stage 1* but skipped in *Stage 2*.

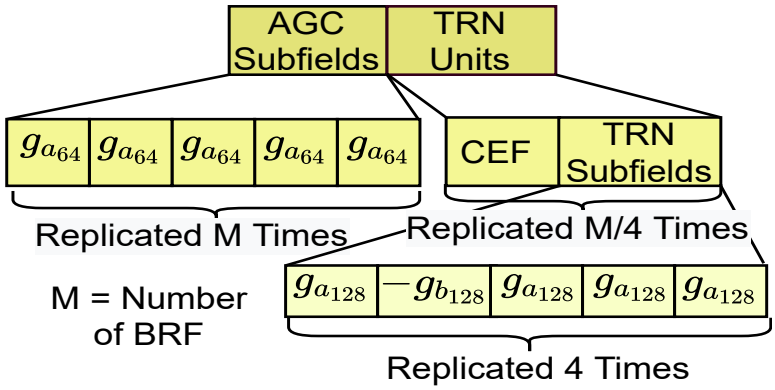

Figure 3.4: Expanded BRF Structure

3.2 Header and Data Processing

The 802.11ad standard specifies that data and header are modulated over 336 data subcarriers (N_{SD}) per OFDM symbol and transmitted over a minimum of 20 OFDM symbols if the optional BRF fields are used. In our proposed JRC, the number of

OFDM symbols, N_{sym}, will be based on the amount of data to be transmitted as BRF are omitted. An additional OFDM symbol is used (for both standard and JRC) to specify the control information in the header, such as the amount of data transmitted and information regarding the modulation and coding schemes (MCS) which must be subsequently used at the BS-RX and MU-RX to recover the data in $\hat{\mathbf{y}}_{\mathrm{DL}}$ and $\hat{\mathbf{y}}_{\mathrm{UL}}$ respectively. Based on the specifications, the header must be modulated with quadrature phase shift keying with $3/4$ coding rate (1 parity bit for every 3 data bits). The standard supports the BPSK, QPSK, 16-bit QAM, and 64-bit QAM modulations and $1/2$, $3/4$, $5/8$, and $13/16$ coding rates for the data. In this work, we use the same MCS for both data and header for simplicity. The header and data are processed as shown in Fig.3.5. In QPSK modulation, two data bits are required

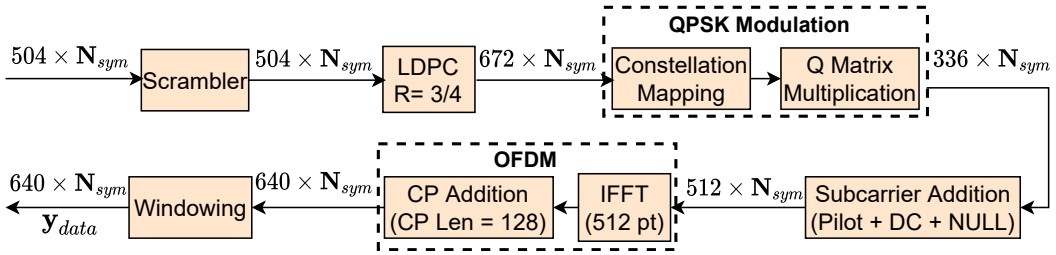

Figure 3.5: Header and data processing

to be mapped to each of the 336 data subcarriers corresponding to a single OFDM symbol. At a $3/4$ coding rate, this corresponds to $3/4 \times 2 \times 336 = 504$ bits per OFDM symbol per packet. If the number of data bits is less than an integral multiple of 504, appropriate zero padding is done. Let the data bits to be transmitted be $\mathbf{y}^{(b)}_{data}[1,q], \mathbf{y}^{(b)}_{data}[2,q], \cdots, \mathbf{y}^{(b)}_{data}[504,q]$ where $q = 1, 2, \cdots, N_{sym}$ and the header bits are denoted as $\mathbf{y}^{(b)}_{header}[1], \mathbf{y}^{(b)}_{header}[2], \cdots, \mathbf{y}^{(b)}_{header}[504]$ Each block of 504 data bits are sequentially passed through a scrambler which is a linear feedback shift register as shown in Fig. 3.6. The first seven bits of the header provide a unique scrambler initialization key to enable bit recovery at the receiver. The scrambling operation can be given by

$$\mathbf{y}^{(b)}_{scrambler}[i,q] = \mathbf{y}^{(b)}_{header}[4] \oplus \mathbf{y}^{(b)}_{header}[7] \oplus \mathbf{y}^{(b)}_{data}[i,q] \qquad i = 1, 2, \cdots, 504 \tag{3.6}$$

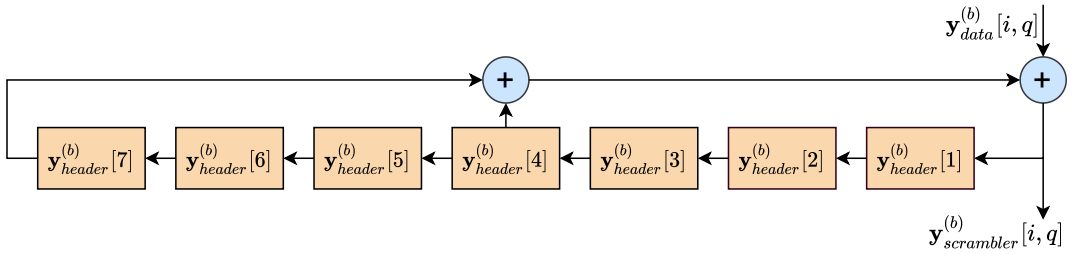

Figure 3.6: Scrambler

The scrambled bits, $\mathbf{y}^{(b)}_{scrambler}$, are then passed through a low density parity check (LDPC) encoder with the $3/4$ code rate. The standard specifies a parity check matrix, $\mathcal{H}$, for every code rate and gives the code word $\mathbf{y}^{(b)}_{LDPC}[q]$ such that data bits followed by parity bits of a single OFDM symbol such that $\mathcal{H}\mathbf{y}^{(\mathbf{b})}_{\mathbf{LDPC}}[\mathbf{q}]^{\mathbf{T}} = 0$. Thus, the LDPC encoded code word is given by

$$\begin{aligned}\mathbf{y}^{(b)}_{LDPC}[q] = [\mathbf{y}^{(b)}_{scrambler}[1,q], \mathbf{y}^{(b)}_{scrambler}[2,q], \cdots, \mathbf{y}^{(b)}_{scrambler}[504,q], \\ \mathbf{y}^{(b)}_{parity}[1,q], \mathbf{y}^{(b)}_{parity}[2,q], \cdots, \mathbf{y}^{(b)}_{parity}[168,q]];\end{aligned} \tag{3.7}$$

After LDPC encoding, each frame has 672 bits which are then modulated into the QPSK WLAN constellation given by

$$\begin{aligned}\mathbf{y}_{QPSK}[2l,q] &= \frac{[(2\times \mathbf{y}_{QPSK}[4l,q]-1) + j(2\times \mathbf{y}_{QPSK}[4l+2,q]-1)]}{\sqrt{2}} \\ \mathbf{y}_{QPSK}[2l+1,q] &= \frac{[(2\times \mathbf{y}_{QPSK}[4l+1,q]-1) + j(2\times \mathbf{y}_{QPSK}[4l+3,q]-1)]}{\sqrt{2}} \\ & l = 0,1,\cdots,\frac{N_{SD}}{2}-1\end{aligned} \tag{3.8}$$

The modulated symbols are then mapped into pairs of symbols and multiplied with a unit matrix $Q = \frac{1}{\sqrt{5}}\begin{bmatrix}1 & 2\\ -2 & 1\end{bmatrix}$ This is known as *static tone pairing* and given as

$$\begin{aligned}[\mathbf{y}_{STP}[l,q], \mathbf{y}_{STP}[p(l),q]] = Q[\mathbf{y}_{QPSK}[2l+1,q], \mathbf{y}_{QPSK}[2l+1,q]] \\ l = 0,1,\cdots,\frac{N_{SD}}{2}-1,\ \ p(l) = l+\frac{N_{SD}}{2}\end{aligned} \tag{3.9}$$

The outcome of the operations is the 336 modulated complex samples per OFDM symbol, to which additional DC, NULL and pilot symbols are added, resulting in 512 complex symbols. This is called *sub-carrier mapping* which is done as specified in the standard [33]. The sub-carrier mapped data for the q^{th} OFDM symbol is denoted by $\mathbf{y}_{SMap}[q]$. Next, OFDM modulation is performed comprising of 512-IFFT and 128-length cyclic prefix (CP) addition. The final modulated signal is given as

$$\begin{aligned}\mathbf{y}_{data}[mT_s,q] = \frac{\sum_{k=\frac{-N_{SD}}{2}}^{\frac{N_{SD}}{2}} \mathbf{y}_{SMap}[q] exp(j2k\pi\Delta f(mT_s - T_{GI}))}{\sqrt{N_{Tones}}} \\ m = 1,2,\cdots,512\end{aligned} \tag{3.10}$$

The complete data packet is formed by appending each OFDM symbol one after the other given as

$$\begin{aligned}\mathbf{y}_{data}[mT_s] = \sum_{q=1}^{N_{sym}} \mathbf{y}_{data}[mT_s,q](mT_s - (q-1)T_{sym}) \\ m = 1,2,\cdots,512\times N_{sym}\end{aligned} \tag{3.11}$$

Header is also generated in the same way while keeping $q = 1$ and it is denoted as $\mathbf{y}_{header}$.

3.3 Windowing

Weighted overlap-and-add (WOLA) windowing is performed on the OFDM modulated header and data to control the out-of-band emission [36]. Each OFDM symbol is extended for the length $T_{TR}/2$ on either side. The extended symbol is shaped on the edges using raised cosine filter whose coefficients are given by

$$win_{RC}[mT_s, q] = \begin{cases} \sin^2\left(\frac{\pi}{2}\right)\left(\frac{1}{2} + \frac{mT_s}{T_{TR}}\right); & \frac{-T_{TR}}{2} < mT_s \leq \frac{T_{TR}}{2} \\ 1; & \frac{T_{TR}}{2} < mT_s \leq T - \frac{T_{TR}}{2} \\ \sin^2\left(\frac{\pi}{2}\right)\left(\frac{1}{2} - \frac{mT_s - T}{T_{TR}}\right); & \frac{T - T_{TR}}{2} < mT_s \leq \frac{T + T_{TR}}{2} \end{cases} \tag{3.12}$$

The coefficients are multiplied with each OFDM symbol and the extended part of each symbol is overlapped with the next OFDM symbol as shown in Fig. 3.7, making the length of each OFDM symbol as T again. In the end, a scheduler combines the

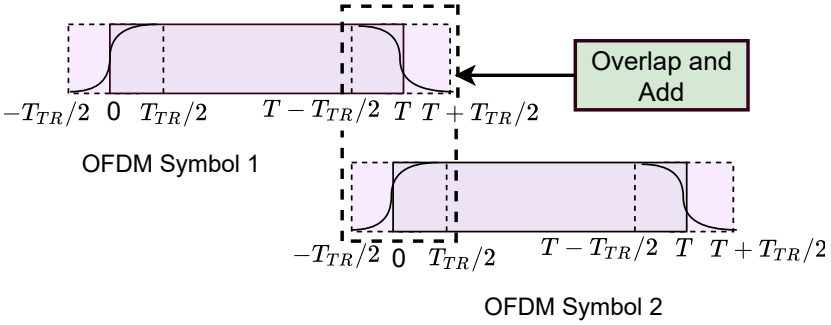

Figure 3.7: Header and data processing

header and data with preamble, and BRF samples to form the packet which is then further processed by DFE and AFE.

3.4 RF Chain

Both the radar signal and the communication signals are converted from digital to analog as shown in

$$\mathbf{x}_{\mathrm{p}}(t) = \sum_{m=0}^{M'} \mathbf{x}_{\mathrm{p}}[mT_s]\delta\left(t - mT_s\right), \tag{3.13}$$

$$\mathbf{y}_{\mathrm{DL}}(t) = \sum_{m=0}^{M} \mathbf{y}_{\mathrm{DL}}[mT_s]\delta\left(t - mT_s\right). \tag{3.14}$$

Here $M' = 768$ (512 Golay samples upsampled by a factor of 1.5) indicates the number of samples within the radar signal which remains fixed since it is independent of data. The number of samples within $\mathbf{y}_{DL}$ varies based on the amount of data to be transmitted and the corresponding N_{sym} OFDM symbols. These signals are then

amplified such that energy E_s is imparted to each symbol. The amplifier output is convolved with a root raised cosine transmit shaping filter, $\mathbf{h}_T$, and then upconverted to the carrier frequency f_c (60GHz) as shown in

$$\mathbf{x}_{\mathrm{p}_{up}}(t) = \sqrt{E_s}\,(\mathbf{x}_{\mathrm{p}}(t) * \mathbf{h}_T(t))\,e^{+j2\pi f_c t} \tag{3.15}$$

$$\mathbf{y}_{\mathrm{DL}_{up}}(t) = \sqrt{Es}\,(\mathbf{y}_{\mathrm{DL}}(t) * \mathbf{h}_T(t))\,e^{+j2\pi f_c t}. \tag{3.16}$$

Then the signals are transmitted through analog beamforming through an N_{BS} element uniform linear array after application of the antenna weight vector, $\mathbf{w}_{BSTX} \in \mathcal{C}^{N_{BS}\times 1}$, as shown in

$$\mathbf{X}_{p_{up}}(t) = \mathbf{w}_{BSTX}\,\mathbf{x}_{\mathrm{p}_{up}}^{T}(t), \tag{3.17}$$

$$\mathbf{Y}_{DL_{up}}(t) = \mathbf{w}_{BSTX}\,\mathbf{y}_{\mathrm{DL}_{up}}^{T}(t). \tag{3.18}$$

The above process is repeated till all the P radar packets are transmitted followed by the communication packets after a guard time interval. In *Stage-1*, the antenna weight vector (AWG) is chosen to support a quasi-omnidirectional beam. At the end of *Stage-1*, when θ of the MU is determined, then the AWV is selected to support a directional beam along θ.

3.5 Analog Beamforming

In this work, we have used phased array implementation to determine the weights of the antennas corresponding to the direction of target, θ, determined by beam training, in case of standard architecture and by RSP in case of JRC. The weight of i^{th} antenna element is given by

$$W[i] = exp\left(\frac{j2\pi f_c(i-1)d\sin\theta}{c}\right);\;\; i = 1, 2, \cdots, N_{TX} \tag{3.19}$$

Here, c is speed of light and d is spacing between two antenna elements known as inter-element spacing.

The signals are transmitted as shown

$$\mathbf{X}_{p_{up}}(t) = \mathbf{W}\,\mathbf{x}_{\mathrm{p}_{up}}^{T}(t), \tag{3.20}$$

$$\mathbf{Y}_{DL_{up}}(t) = \mathbf{W}\,\mathbf{y}_{\mathrm{DL}_{up}}^{T}(t). \tag{3.21}$$

Thus, we complete the design of the transmitted signal. The above discussed parts are implemented on Matlab using the floating point architecture and hence we call it as *software prototype*. In the next chapter, we map the above architecture on fixed point which is compatible with Xilinx 7 series FPGA.

Chapter 4: Fixed-Point Architecture of JRC Transmitter

Matlab's Simulink provides a platform for the implementation of algorithms in a block-level environment that is closer to the actual hardware implementation. The virtual model created through the Simulink workflow allows easy validation and is useful for rapid prototyping. The tool also provides an HDL coder which generates the codes in a high-level language such as C, C++, Verilog, etc., that can be deployed directly on an field programmable gate array (FPGA). The implementation of the algorithms on a synthesizable hardware model is typically done using the fixed point architecture. There are two configurations to synthesize a logic in the HDL coder: Programmable Logic (PL) and Processing System (PS). In PL configuration, the processing is done sample-based, i.e., processing one sample at a time on a certain frequency, and it also enables parallel implementation of certain parts of the logic. In PS configuration, frame-based processing is done, and hence the implementation of logic is done serially.

In this chapter, we discuss the implementation of the 802.11ad based JRC transmitter, for generating $\mathbf{y}_{DL}$ (omitted BRF fields) on the Xilinx ZC706 FPGA using Matlab's Simulink HDL coder. The purpose of the implementation is to understand the extent of differences that arises when we shift the architecture from 64-bit double precision in Matlab to a fixed point architecture with less number of bits. We have made the design in the PL configuration at the sampling frequency fs_{OFDM}. The detailed implementation of the data chain within the transmitter is shown in Fig.4.1. Every

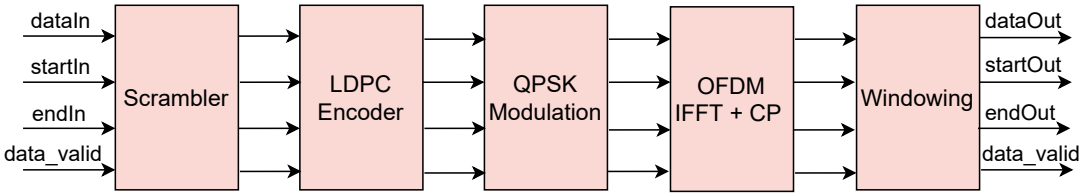

Figure 4.1: Data Chain

subsystem has four inputs and four outputs. First input, *dataIn*, denotes the data that is entering each subsystem, and after the processing, the modified data is *dataOut*. Next input is *startIn* which marks the starting of data corresponding to every OFDM symbol in every subsystem by settling its value as 1, and it is set to 0 otherwise. Corresponding to the input, *startOut* represents the starting point of the OFDM symbols after the processing of the particular subsystem. Next input-outputs, *endIn* and *endOut* is same as *startIn* and *startOut* which marks the ending of each OFDM symbols. It is also used to reset subsystems like LDPC encoder, OFDM modulation, and windowing. These two inputs are very important as they help in tracking the changing sizes of data in every subsystem. The last input is the *data_valid*, which is set to 1 for the significant data and separates it from the unwanted data. It is the control signal for the entire architecture which is to be implemented on FPGA. The preamble and

header are implemented in Matlab, and their final values are stored in a look-up table (LUT) along with the corresponding valid signals. The scheduler combines data with header and preamble as shown in 4.2 and generates the complete transmitted packet for JRC. For the implementation of block-level design on FPGA, an HDL workflow

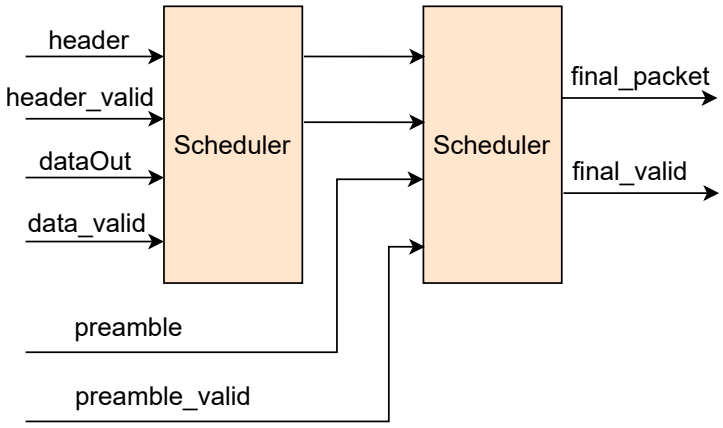

Figure 4.2: Scheduling of the preamble, header and data to generate the waveform.

advisor converts the design into its corresponding the bit stream, which is loaded on the Xilinx ZC706 FPGA board for further testing. Through this process the design is mapped on the FPGA board, and it generates reports regarding the utilization of resources and power for the given model. These reports are analyzed further to decide upon the optimum word length for a particular implementation.

Chapter 5: Results

In the chapter, we present the numerical results for the beam alignment of standard architecture and the two versions of JRC architecture. We also present the simulation results that verify the functional correctness of the mapping of JRC transmitter architecture from Matlab to FPGA.

5.1 Timing Analysis

In this section, we compare the time taken for beam alignment - the duration of *Stage-1* - for the standard IEEE 802.11ad and the two versions of the proposed JRC. The timing analysis is carried out based on the architecture presented in Chapter 2 and the results are reported in Table.5.1.

For both versions of the JRC and the standard architectures, we assume that the BS and MU have a ULA of 32 beams and 4 beams, respectively. The total beam alignment time is based on the number of packets, their duration as well as the processing time of packets which are of the order of milliseconds. In this work, all the processing is carried out in floating-point in MATLAB 2021a on an Intel Core i7 processor with 128 GB RAM. The one-way and two-way propagation times for communication and radar are neglected since they are comparably much shorter (of the order of nanoseconds) over the short ranges of the MU with respect to the BS than the signal lengths and signal processing times.

In standard protocol, $\mathbf{y}_{DL}$ consists of 32 BRF fields in addition to the preamble, header, and data to support beam alignment at the BS. This results in a packet length of 26.3μs duration for $N_{sym} = 20$ data symbols which is the minimum specified by the protocol. This packet is transmitted 4 times with an inter-packet guard spacing of $1\mu s$ to support beam alignment at MU. The receiver communication processing time for one packet is 16ms, where the best beams for the MU and BS are computed. This information is then communicated through the subsequent $\mathbf{y}_{UL}$ transmitted over the MU's best beam to the BS where it is processed. Then, the next $\mathbf{y}_{DL}$ is transmitted over BS's best beam and received by the MU's best beam in *Stage-2*. The overall beam alignment duration for BS and MU are 80.1ms and 64ms, respectively. The *Stage-1* alignment time is computed by the total time required for both BS and MU beam alignment (the greater of the two times). Note that in standard beam alignment, the overall duration is a function of the communication packet length and hence the number of OFDM data symbols. Also, the packets are long since they must include the BRF fields for all possible beams from the BS and repeated for all possible beams of the MU. The recovery of data bits from the received data packet is computationally intensive and hence requires a long time. After the data bit recovery from each packet, the BRF fields are processed for the correlation gains, generating an $M \times N$ matrix. Finally, the $(m, n)^{th}$ element of the matrix with the highest correlation gain where m and n provide the best beam among the M BS beams and N MU beams, respectively. All the above factors result in a long beam alignment phase.

Table 5.1: Timing analysis for beam alignment for Standard, JRC *Version-1*, and JRC *Version-2*

Signals	Signal Processing	Standard			JRC *Version- 1*			JRC *Version-2*		
		D	P	T	D	P	T	D	P	T
DL Packet $\mathbf{y}_{DL}$ (in μs)		26.3	4	105.2	4.5	1	4.5	4.5	4	18
UL Packet $\mathbf{y}_{DL}$ (in μs)		4.5	1	4.5	9.82	1	9.82	-	-	-
Comm Idle Time (in μs)		1	3	3	-	-	-	1	3	3
Radar Waveform $\mathbf{x}_{Dp}$ (in μs)		-	-	-	0.29	2	0.58	0.29	2	0.58
Pulse Repetition Interval T_{PRI} (in μs)		-	-	-	0.29	2	0.58	0.29	2	0.58
	RCP on $\hat{\mathbf{y}}_{DL}$ (in ms)	16	4	64	16	2	32		-	-
	RCP on $\hat{\mathbf{y}}_{UL}$ (in ms)	16	1	16	16	1	16	-	-	-
	Receive Preamble Correlation $\hat{\mathbf{y}}_{DL}$ (in ms)	-	-	-	-	-	-	-	-	4.5
	Radar/Comm Detection Unit (in ms)	-	-	-	2.5	2	5	2.5	1	2.5
	Preamble Bits Extraction (in ms)	-	-	-	1.6	-	1.6	1.6	-	1.6
	RSP on $\hat{\hat{\mathbf{x}}}_p, p = 1, 2$ (in ms)	-	-	-	16	-	16	16	-	16
Total time for beam alignment at BS		64+16+0.10 =80.1ms			16+2.5+1.6 =20.1ms			16+2.5+1.6 =20.1ms		
Total time for beam alignment at MU				64 ms			16+16+2.5 =34.5ms			4.5 ms
Total time for completion of *Stage 1*				80.1 ms			34.5 ms			20.1 ms

D: Duration of packet P: Number of packets required T: Total duration

Next, we consider the *Stage-1* beam alignment duration of the JRC. The two symbols of radar waveform ($\mathbf{x}_1$ and $\mathbf{x}_2$) are each of very short duration ($0.29\mu s$) since they consist of only 512 samples and are transmitted ahead of a $\mathbf{y}_{DL}$ packet with $N_{sym} = 10$ symbols of data (without BRF fields). The T_{PRI} for each radar signal is $0.58\mu s$, which results in a maximum detectable range of approximately 87m. The reflected received signals, $\hat{\hat{\mathbf{x}}}_p, p = 1, 2$, are detected in the radar-communication detection unit and subsequently processed to estimate the MU's range, Doppler, and azimuth angle within a duration of 16ms. Hence the total time required at the BS for beam alignment is 20ms. Note that this time requirement is entirely independent of the number of OFDM data symbols that are transmitted in $\mathbf{y}_{DL}$. Further, since the BRF fields are omitted in $\mathbf{y}_{DL}$, the minimum number of OFDM data symbols that must be transmitted in the packet is no longer 20 and instead directly based on the amount of data that is to be transmitted. The JRC is only included in the BS and not in the MU. Hence, we present two different versions of beam alignment at the MU.

In JRC *Version-1*, $\mathbf{y}_{DL}$ is first received at MU with a quasi-omnidirectional beam. Once the data are processed, the MU transmits the $\mathbf{y}_{UL}$ with four BRF fields, such that each field is transmitted through a different directional beam. The duration of this packet is $9.82\mu s$ to account for $N_{sym} = 20$ symbols of data along with the BRF fields. The received $\hat{\mathbf{y}}_{UL}$ is processed at the BS to determine the best beam of the MU. The duration of the processing is 16ms. Once the best beam is determined, the information is communicated to the MU through the next $\mathbf{y}_{DL}$. Hence, the total duration for beam alignment at MU is 50.1ms which is shorter than the standard. In JRC *Version-2*, the BS sends four consecutive $\mathbf{y}_{DL}$ packets. Each of these packets consists of $N_{sym} = 10$ OFDM symbols and zero BRF fields, hence of a duration of $4.5\mu s$. The MU receives each packet through the corresponding beam, one at a time. All four data packets are processed to estimate the best possible beam at the MU, and the time taken for beam alignment at MU is 4.5ms. The short processing time is because the best beam is determined using the parallel correlation operation on the Golay sequences of the preamble of the multiple packets.

From this timing analysis, it is evident that the JRC based architecture provides faster beam alignment than the standard for the same number of beams at BS and MU. This can be attributed to two factors - first, the reduction of the packet duration due to the omission of the BRF fields due to radar based beam alignment at the BS. This also reduces the total number of packets that have to be transmitted to support the beam alignment at the MU (especially in *Version-1*). Second, digital beamforming and subsequent radar signal processing at the BS-RX support the detection and localization of the MU. This becomes even more advantageous when there are multiple MU in the channel since the above beam refinement protocol for multiple MU can be carried out in parallel since the radar can detect multiple targets. This is not possible with the standard protocol.

5.2 Comparison of Hardware-Software Prototype Results

In this section, we discuss the effect of the word length of fixed point architecture when compared to floating point architecture. These results are to verify that the algorithm that we formulated in floating point architecture during the software simulation for JRC is mapped appropriately on the fixed point architecture for the hardware simulation in terms of functionality. Here, we study the effect of different word lengths and how the results show deviation when we fix the number of bits available for representing integer and decimal parts of processed data. We present this analysis through two types of results, *BER Vs. SNR plots* and *Power spectral density*.

5.2.1 Power Spectral Density (PSD)

PSD is a measure of determining the distribution of signal power across various frequency components. Here, we plot the magnitude of power in a logarithmic scale across the normalized frequency components. This shows out-of-band emission (OOB) for the transmitted data and hence verifies the functionality of the transmitter in different configurations. We have generated the PSD for the transmitter for different word lengths and benchmarked it against the Matlab implemented transmitter. The plots for PSD for different word lengths is shown in Fig. 5.1. In the given, we

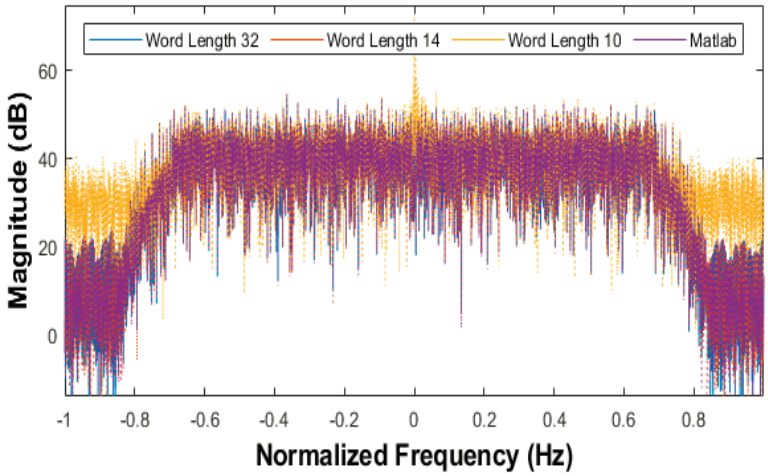

Figure 5.1: Power spectral density for different word length

can observe that the PSD for Matlab implemented transmitter is coinciding with the transmitter implemented with a word length (WL) of 14 and 32 bits. On the other hand, the implementation of a transmitter with WL 10 bits shows greater OOB. This occurs due to the insufficient number of bits available to represent the non-binary data, i.e., the data after QPSK modulation. Hence, we say that the transmitter with WL 14 and 32 bits are functionally correct as compared to WL 10 bits. Further verification of the accuracy of the transmitter with WL 32 is discussed through the bit error rates (BER) over different values of signal-to-noise ratio (SNR) values in the next subsection.

5.2.2 BER Vs SNR

This result is to test the performance of the transmitter under various SNR. For this, we have passed the multiple packets data bits equivalent to 10 OFDM symbols through both the transmitters, the one implemented on Matlab and the one implemented on fixed point architecture when the WL chosen for representing the non-binary data, i.e., the QPSK modulated data is represented using 14, 20 and 32 bits. The transmitted data is then passed through the IEEE 802.11ad receiver that extracts the data bits from the data it receives. To verify the functionality, we have considered a Fri's free channel where signal attenuation is due to the distance between transmitter and receiver, which is taken as the maximum possible range detectable by radar which is 80m. The additive white Gaussian noise (AWGN) is added to the radar/communication signal. The BER Vs. SNR plot is given in Fig. 5.2. From

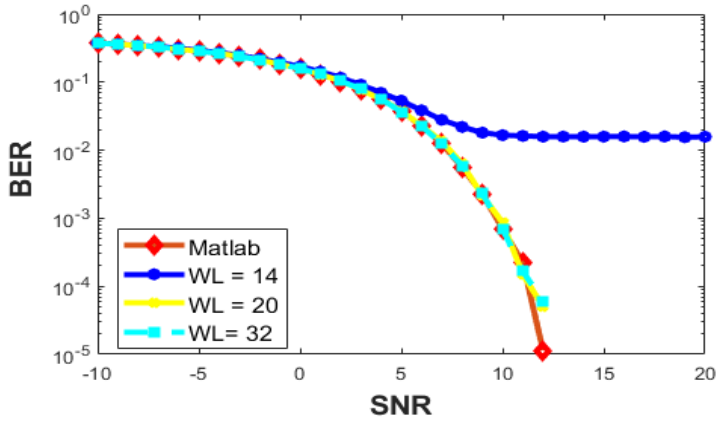

Figure 5.2: BER Vs SNR plot for Floating Point and Fixed Point Architecture

the figure, we can see that even when the PSD for WL 14 coincides with the Matlab transmitter, it does not give correct performance for BER calculation. For the WL 20 and 32 the plots coincide with each other for most of the values of the SNR but deviates slightly after a point. This is because we are limiting the number of bits required for representation of data in the transmitter. Since the deviation is very small, it confirms the correctness of the functionality of the transmitter on the fixed point architecture. As we increase the WL in the implementation, the accuracy of the system increases, but the resources required also increase. For example, from moving the architecture from WL 20 to WL 32 the number of DSP blocks increases by a factor of 3.62 and block RAMs increases by a factor of 9.22. Hence, we need to determine the optimum word length which is the smallest WL that gives the same functionality as the Matlab implemented transmitter.

Hence, we can conclude that the selection of word length is very critical in determining the functionality of the transmitter. If the word length is too less, then the transmitter is functionally incorrect, whereas a larger word length leads to increased utilization of resources. The resource utilization can be studied from the reports that are generated during bit-stream generation. From the analysis of functionality and resource utilization we can decide upon optimum word length.

Chapter 6: Conclusion and Future Scope

We have implemented the software prototype of an IEEE 802.11ad based JRC wireless transmitter for enabling mmW communications between BS and MU. The radar functionality within the JRC provides accurate estimates of their angular positions through the range, Doppler, and azimuth processing. This information at the BS enables rapid beam alignment of the communication beams at the BS when compared to the lengthy beam training procedure adopted by the standard protocol. For an example case of a system with 32 beams in the BS and 4 beams in the MU, we demonstrate an improvement in the beam alignment timing by a factor of 4 for the JRC with respect to the standard. The main advantages offered by the JRC are the reduction in the packet lengths and number due to the omission of the beam training fields overhead. We have also implemented the hardware prototype of the transmitter design on the fixed point architecture, and the results with WL 20 are comparable with the 64-bit double precision floating point architecture implemented on Matlab.

Future work is to optimize the hardware prototype configurations to have better performance in terms of reduced latency and utilised resources. The hardware implementation of the receiver communication processing for extraction of data bits is currently under implementation, and we plan to implement radar signal processing on fixed point architecture for a complete hardware prototype for JRC system. We further plan to develop the analog and RF on fixed point architecture and integrate with the digital interface developed on Simulink HDL coder for testing the system level performance. We will also extend our proposed JRC architecture and evaluate its performance for the multiple target scenario and conduct laboratory and field experiments to evaluate the performance of the final prototype.

References

[1] L. Hobert, A. Festag, I. Llatser, L. Altomare, F. Visintainer, and A. Kovacs, "Enhancements of V2X communication in support of cooperative autonomous driving," *IEEE Communications Magazine*, vol. 53, no. 12, pp. 64–70, 2015.

[2] J. B. Kenney, "Dedicated short-range communications (DSRC) standards in the United States," *Proceedings of the IEEE*, vol. 99, no. 7, pp. 1162–1182, 2011.

[3] A. Asadi, Q. Wang, and V. Mancuso, "A survey on device-to-device communication in cellular networks," *IEEE Communications Surveys & Tutorials*, vol. 16, no. 4, pp. 1801–1819, 2014.

[4] P. Wang, B. Di, H. Zhang, K. Bian, and L. Song, "Cellular V2X communications in unlicensed spectrum: Harmonious coexistence with VANET in 5G systems," *IEEE Transactions on Wireless Communications*, vol. 17, no. 8, pp. 5212–5224, 2018.

[5] J. Choi, V. Va, N. Gonzalez-Prelcic, R. Daniels, C. R. Bhat, and R. W. Heath, "Millimeter-wave vehicular communication to support massive automotive sensing," *IEEE Communications Magazine*, vol. 54, no. 12, pp. 160–167, 2016.

[6] C. Liu, M. Li, S. V. Hanly, I. B. Collings, and P. Whiting, "Millimeter wave beam alignment: Large deviations analysis and design insights," *IEEE Journal on Selected Areas in Communications*, vol. 35, no. 7, pp. 1619–1631, 2017.

[7] J. C. Aviles and A. Kouki, "Position-aided mm-wave beam training under NLOS conditions," *IEEE Access*, vol. 4, pp. 8703–8714, 2016.

[8] Z. Feng, Z. Fang, Z. Wei, X. Chen, Z. Quan, and D. Ji, "Joint radar and communication: A survey," *China Communications*, vol. 17, no. 1, pp. 1–27, 2020.

[9] A. R. Chiriyath, B. Paul, and D. W. Bliss, "Radar-communications convergence: Coexistence, cooperation, and co-design," *IEEE Transactions on Cognitive Communications and Networking*, vol. 3, no. 1, pp. 1–12, 2017.

[10] B. Li and A. P. Petropulu, "Joint transmit designs for coexistence of MIMO wireless communications and sparse sensing radars in clutter," *IEEE Transactions on Aerospace and Electronic Systems*, vol. 53, no. 6, pp. 2846–2864, 2017.

[11] A. F. Martone, K. I. Ranney, K. Sherbondy, K. A. Gallagher, and S. D. Blunt, "Spectrum allocation for noncooperative radar coexistence," *IEEE Transactions on Aerospace and Electronic Systems*, vol. 54, no. 1, pp. 90–105, 2017.

[12] A. Hassanien, M. G. Amin, Y. D. Zhang, and F. Ahmad, "Signaling strategies for dual-function radar communications: An overview," *IEEE Aerospace and Electronic Systems Magazine*, vol. 31, no. 10, pp. 36–45, 2016.

[13] F. Hessar and S. Roy, "Spectrum sharing between a surveillance radar and secondary Wi-Fi networks," *IEEE Transactions on Aerospace and Electronic Systems*, vol. 52, no. 3, pp. 1434–1448, 2016.

[14] Y. Zeng, R. Zhang, and T. J. Lim, "Wireless communications with unmanned aerial vehicles: Opportunities and challenges," *IEEE Communications Magazine*, vol. 54, no. 5, pp. 36–42, 2016.

[15] K. V. Mishra, M. B. Shankar, V. Koivunen, B. Ottersten, and S. A. Vorobyov, "Toward millimeter-wave joint radar communications: A signal processing perspective," *IEEE Signal Processing Magazine*, vol. 36, no. 5, pp. 100–114, 2019.

[16] A. Hassanien, M. G. Amin, E. Aboutanios, and B. Himed, "Dual-function radar communication systems: A solution to the spectrum congestion problem," *IEEE Signal Processing Magazine*, vol. 36, no. 5, pp. 115–126, 2019.

[17] S. S. Ram, S. Singhal, and G. Ghatak, "Optimization of network throughput of joint radar communication system using stochastic geometry," *Frontiers in Signal Processing*, vol. 2, 2022.

[18] C. Sahin, J. Jakabosky, P. M. McCormick, J. G. Metcalf, and S. D. Blunt, "A novel approach for embedding communication symbols into physical radar waveforms," in *2017 IEEE Radar Conference (RadarConf)*, pp. 1498–1503, IEEE, 2017.

[19] M. Jamil, H.-J. Zepernick, and M. I. Pettersson, "On integrated radar and communication systems using oppermann sequences," in *MILCOM 2008-2008 IEEE Military Communications Conference*, pp. 1–6, IEEE, 2008.

[20] F. Liu, L. Zhou, C. Masouros, A. Li, W. Luo, and A. Petropulu, "Toward dual-functional radar-communication systems: Optimal waveform design," *IEEE Transactions on Signal Processing*, vol. 66, no. 16, pp. 4264–4279, 2018.

[21] P. Kumari, J. Choi, N. González-Prelcic, and R. W. Heath, "Ieee 802.11 ad-based radar: An approach to joint vehicular communication-radar system," *IEEE Transactions on Vehicular Technology*, vol. 67, no. 4, pp. 3012–3027, 2017.

[22] L. Zhou and Y. Ohashi, "Efficient codebook-based mimo beamforming for millimeter-wave wlans," in *2012 IEEE 23rd International Symposium on Personal, Indoor and Mobile Radio Communications-(PIMRC)*, pp. 1885–1889, IEEE, 2012.

[23] K. V. Mishra, M. Bhavani Shankar, V. Koivunen, B. Ottersten, and S. A. Vorobyov, "Toward millimeter-wave joint radar communications: A signal processing perspective," *IEEE Signal Processing Magazine*, vol. 36, pp. 100–114, Sept. 2019.

[24] T. Nitsche, C. Cordeiro, A. B. Flores, E. W. Knightly, E. Perahia, and J. C. Widmer, "Ieee 802.11 ad: directional 60 ghz communication for multi-gigabit-per-second wi-fi," *IEEE Communications Magazine*, vol. 52, no. 12, pp. 132–141, 2014.

[25] G. R. Muns, K. V. Mishra, C. B. Guerra, Y. C. Eldar, and K. R. Chowdhury, "Beam alignment and tracking for autonomous vehicular communication using ieee 802.11 ad-based radar," in *IEEE INFOCOM 2019-IEEE conference on computer communications workshops (INFOCOM WKSHPS)*, pp. 535–540, IEEE, 2019.

[26] P. Kumari, S. A. Vorobyov, and R. W. Heath, "Adaptive virtual waveform design for millimeter-wave joint communication-radar," *IEEE Transactions on Signal Processing*, vol. 68, pp. 715–730, 2019.

[27] S. H. Dokhanchi, B. S. Mysore, K. V. Mishra, and B. Ottersten, "A mmwave automotive joint radar-communications system," *IEEE Transactions on Aerospace and Electronic Systems*, vol. 55, no. 3, pp. 1241–1260, 2019.

[28] D. Ma, N. Shlezinger, T. Huang, Y. Shavit, M. Namer, Y. Liu, and Y. C. Eldar, "Spatial modulation for joint radar-communications systems: Design, analysis, and hardware prototype," *IEEE Transactions on Vehicular Technology*, vol. 70, no. 3, pp. 2283–2298, 2021.

[29] P. Kumari, A. Mezghani, and R. W. Heath, "JCR70: A low-complexity millimeter-wave proof-of-concept platform for a fully-digital SIMO joint communication-radar," *IEEE Open Journal of Vehicular Technology*, vol. 2, pp. 218–234, 2021.

[30] J. Pegoraro, J. O. Lacruz, E. Bashirov, M. Rossi, and J. Widmer, "RAPID: Retrofitting IEEE 802.11 ay access points for indoor human detection and sensing," *ArXiv Preprint arXiv:2109.04819*, 2021.

[31] B. Drozdenko, M. Zimmermann, T. Dao, K. Chowdhury, and M. Leeser, "Hardware-software codesign of wireless transceivers on zynq heterogeneous systems," *IEEE Transactions on Emerging Topics in Computing*, vol. 6, no. 4, pp. 566–578, 2017.

[32] Y. M. Tsang, A. S. Poon, and S. Addepalli, "Coding the beams: Improving beamforming training in mmwave communication system," in *2011 IEEE Global Telecommunications Conference-GLOBECOM 2011*, pp. 1–6, IEEE, 2011.

[33] "IEEE Std 802.11™-2016, IEEE standard for information technology—telecommunications and information exchange between systems—local and metropolitan area networks—specific requirements—Part 11: Wireless LAN medium access control," p. 3534, 2016.

[34] P. Kumari, S. A. Vorobyov, and R. W. Heath, "Adaptive virtual waveform design for millimeter-wave joint communication–radar," *IEEE Transactions on Signal Processing*, vol. 68, pp. 715–730, 2020.

[35] G. Duggal, S. Vishwakarma, K. V. Mishra, and S. S. Ram, "Doppler-resilient 802.11 ad-based ultrashort range automotive joint radar-communications system," *IEEE Transactions on Aerospace and Electronic Systems*, vol. 56, no. 5, pp. 4035–4048, 2020.

[36] N. Agrawal, S. J. Darak, and F. Bader, "Spectral coexistence of LDACS and DME: Analysis via hardware software co-design in presence of real Channels and RF impairments," *IEEE Transactions on Vehicular Technology*, vol. 69, pp. 9837–9848, Sept. 2020.